

UCLA

UCLA Previously Published Works

Title

Potential impacts on regional climate due to land degradation in the Guizhou Karst Plateau of China

Permalink

<https://escholarship.org/uc/item/0b03r4r2>

Journal

Environmental Research Letters, 8(4)

ISSN

1748-9318

Authors

Gao, Jiangbo
Xue, Yongkang
Wu, Shaohong

Publication Date

2013-12-01

DOI

10.1088/1748-9326/8/4/044037

Peer reviewed

Potential impacts on regional climate due to land degradation in the Guizhou Karst Plateau of China

This content has been downloaded from IOPscience. Please scroll down to see the full text.

2013 Environ. Res. Lett. 8 044037

(<http://iopscience.iop.org/1748-9326/8/4/044037>)

View [the table of contents for this issue](#), or go to the [journal homepage](#) for more

Download details:

IP Address: 159.226.111.166

This content was downloaded on 13/02/2014 at 06:22

Please note that [terms and conditions apply](#).

Potential impacts on regional climate due to land degradation in the Guizhou Karst Plateau of China

Jiangbo Gao¹, Yongkang Xue^{2,3} and Shaohong Wu¹

¹ Institute of Geographic Sciences and Natural Resources Research, Chinese Academy of Sciences, Beijing 100101, People's Republic of China

² Department of Geography, University of California, Los Angeles, CA 90095-1524, USA

³ Department of Atmospheric and Oceanic Sciences, University of California, Los Angeles, CA 90095-1524, USA

E-mail: wush@igsnr.ac.cn

Received 27 June 2013

Accepted for publication 1 November 2013

Published 21 November 2013


Online at stacks.iop.org/ERL/8/044037

Abstract

The possible regional climatic effects of land condition change in the Guizhou Karst Plateau (GKP), which has experienced serious Karst Rocky Desertification (KRD) in the past decades, were investigated in this study using the Weather Research and Forecasting (WRF) regional climate model. It was shown that when compared with validation datasets, the WRF showed a high ability to downscale NCEP-DOE Reanalysis-2, which provided the initial and lateral boundary conditions for WRF, especially for the precipitation simulation.

After land degradation over the GKP, the net radiation and evaporation were reduced mainly within the desertification area, consistent with the reduction in rainfall and the increase in surface temperature there. The southwest monsoon flow from the Bay of Bengal was weakened over the adjacent area to the northeast, influencing the East Asian summer monsoon. Meanwhile, the weaker low-layer anti-cyclone and the stronger horizontal convergence enhanced vertical motion in the southeastern coastal areas. Furthermore, owing to the decreased surface heating in the degradation experiment, the lifting over the GKP and neighboring regions to the east was limited, which resulted in a reduced rainfall within the GKP and strengthened the ascending motion downstream over 114°–122°E. Such circulation differences favored an increase in moisture flux and clouds, thereby causing more precipitation in coastal areas of southeast China.

Keywords: Karst Rocky Desertification, Guizhou Karst Plateau, climatic effects, WRF model, physical processes

 Online supplementary data available from stacks.iop.org/ERL/8/044037/mmedia

1. Introduction

During the past three decades, with the increasing reports of land cover change (LCC) in many regions, the feedbacks

of LCC to the climate have attracted widespread attention (Bounoua *et al* 2002, Xue *et al* 2004, Gibbard *et al* 2005, McAlpine *et al* 2007, Pitman *et al* 2009, Wang *et al* 2013, Zhang *et al* 2013). Previous studies showed that atmosphere and terrestrial ecosystem interactions are as important as atmospheric dynamics and composition, ocean circulation, and solar orbit perturbations in climate variations (Pielke *et al* 1998). Most research has concluded that the effect of LCC



Content from this work may be used under the terms of the [Creative Commons Attribution 3.0 licence](http://creativecommons.org/licenses/by/3.0/). Any further distribution of this work must maintain attribution to the author(s) and the title of the work, journal citation and DOI.

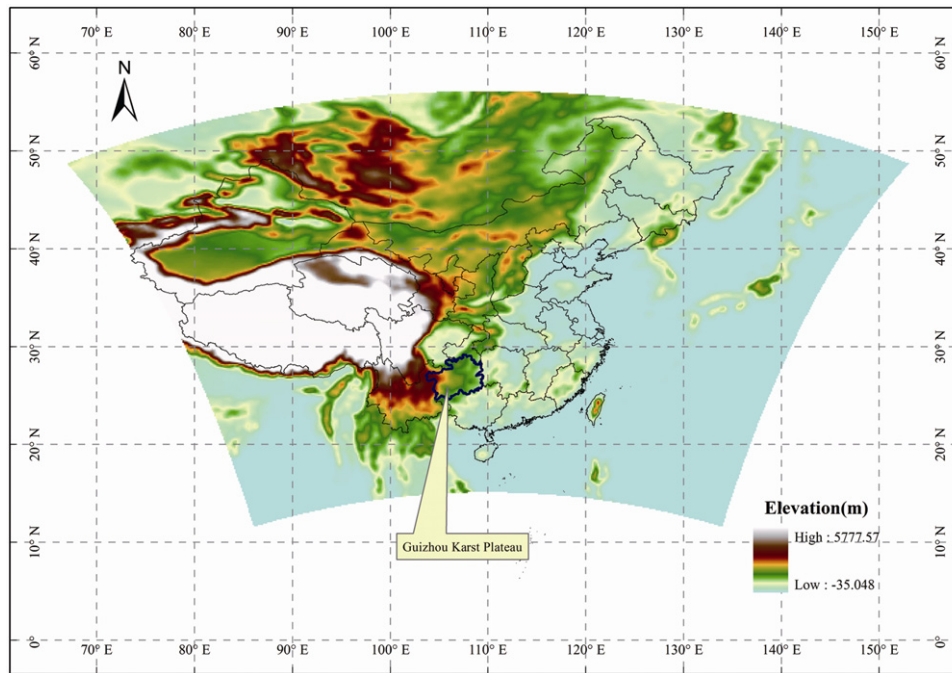


Figure 1. Location of the Guizhou Karst Plateau (GKP) and the experimental domain (shaded). This domain covers the areas that are important for the development of the East Asian summer monsoon.

on regional climate is stronger than that on global climate. For example, based on two vegetation maps with different land cover conditions over the Tibetan Plateau (TP), Li and Xue (2010) showed that LCC from vegetated land to bare ground led to the weaker summer monsoon circulation and the decreased precipitation in the southeastern TP. Furthermore, Zuo *et al* (2011) pointed out that increased vegetation in the southern TP cannot only influence the TP climate, but also weaken the East Asian summer monsoon, and consequently enhance summer rainfall in southern and northern China.

The Guizhou Karst Plateau (GKP), located in the center of the southwestern Karst area in China (figure 1), was selected as the study area. Under the conditions of widely distributed carbonate and a warm–humid monsoon climate, bare limestone regions account for about 73% of the total area (Xiong *et al* 2002). Due to the fragile ecosystems, the rapid growth of population and unsuitable land use (e.g., cultivating land at the cost of destroying forests and/or on slopes of over 25°), Karst Rocky Desertification (KRD) has become the most serious pressure in this region since the 1950s (Yuan 1997, Wang *et al* 2004, Huang and Cai 2006). An interpretation from remote sensing revealed that KRD land in the GKP covers over 20% of the total area (Wang *et al* 2004). The rocky desertification rate of 2.5×10^4 km² in southwestern China equals the desertification rate in the sandy loess of northwestern China. Based on both satellite images and field observations, Xiong *et al* (2002) extracted the spatial pattern of KRD, and concluded that rocky desertification in the GKP exhibits the three characteristics of severe degree, large area and high risk.

Until now, the threats of KRD to soil erosion, soil moisture, productivity of agriculture, forestry and livestock

husbandry, local poverty, and even silting up in the lower reaches of the Yangtze and Pearl rivers have been fully discussed (Wang *et al* 2004). Possible responses of vegetation to climate change were also noted by statistical methods (Gao *et al* 2012). Although the surface heating over the GKP is significant due to the high altitude, the feedback of vegetation cover to climate, including the downstream climate effects, and the relevant biophysical processes remain unknown.

Compared with GCMs with their coarse resolution, meso-scale models may be able to more realistically assess the consequences of LCC at local scales. Therefore, the WRF (Weather Research and Forecasting Model) regional climate model (RCM) (Skamarock *et al* 2008), coupled with the simplified simple biosphere (SSiB) model (Xue *et al* 1991, 2001), was applied to answer the question: can land degradation, which has occurred and will continue in the GKP, influence regional climate? The relevant physical processes, including biophysical feedback of vegetation cover to atmospheric circulation, were addressed.

The purpose of this letter is to preliminarily assess the potential influence of KRD over the GKP on the major climate features in summer (June, July and August, JJA) for East Asia. Dynamic downscaling of monsoon precipitation over East Asia is a challenging task due to the complexity in the regional climate (Gao *et al* 2011), so a better understanding of the various land–atmosphere interactions could be helpful in simulating the monsoonal climate in East Asia. In this letter, section 2 describes the experimental design based on the coupled WRF/SSiB model. Section 3 discusses the model performance of WRF/SSiB and the climatic effects of land degradation. Finally, concluding remarks are given in section 4.

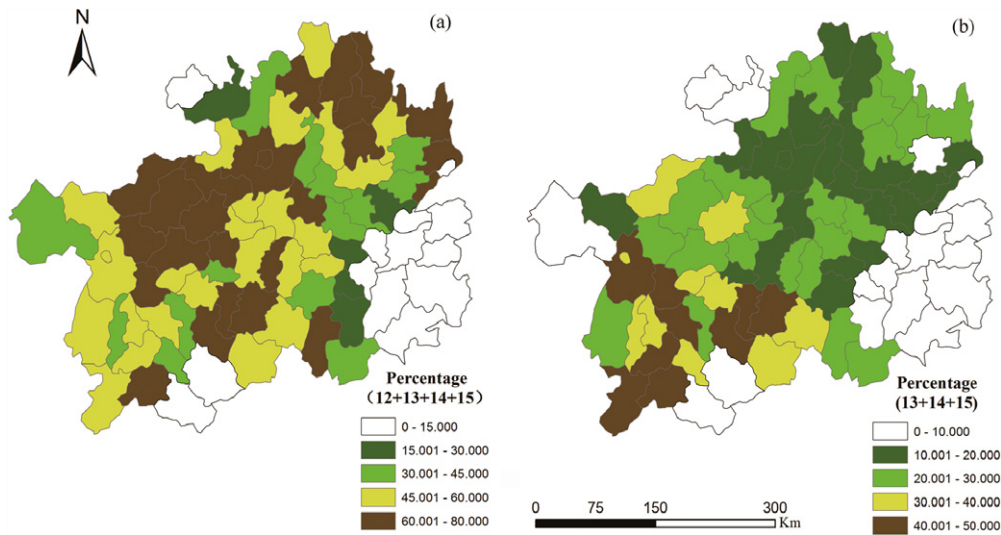


Figure 2. The percentage of total area with different degrees of rocky desertification for counties over the GKP: (a) 12 + 13 + 14 + 15; (b) 13 + 14 + 15. 12: potential desertification; 13: mild desertification; 14: moderate desertification; 15: severe desertification.

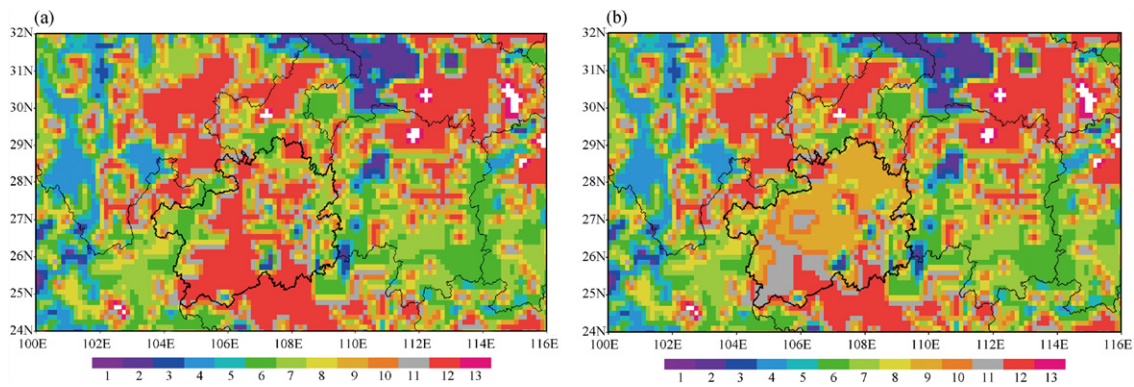


Figure 3. SSiB vegetation cover types: (a) original vegetation map used in case C; (b) vegetation map with land degradation used in case D. Type 1, tropical rainforest; type 2, broadleaf deciduous trees; type 3, broadleaf and needleleaf trees; type 4, needleleaf evergreen trees; type 5, needleleaf deciduous trees; type 6, broadleaf trees with ground cover; type 7, grassland; type 8, broadleaf shrubs with ground cover; type 9, broadleaf shrubs with bare soil; type 10, dwarf trees with ground cover; type 11, bare soil; type 12, crops; type 13, permanent ice. The GKP is bounded by a heavy border.

2. Data and methods

Employing the coupled WRF/SSiB model, we designed two experiments to explore the impacts of LCC over the GKP on regional climate: one used the original SSiB vegetation map, which represents the natural vegetation distribution (figure 3(a)), called case C, and the other, referred to as case D, is a modification of the former one according to Xiong *et al* (2002). Firstly, based on the spatial pattern of rocky desertification at a finer patchy scale from Xiong *et al* (2002), statistical results concerning the percentage of areas with different degrees of desertification in every county of the GKP are displayed in figure 2. Figure 2(a) shows the percentage of the total area with potential desertification, mild desertification, moderate desertification and severe desertification, while figure 2(b) represents the same percentages as figure 2(a) but excluding potential desertification. Secondly, the SSiB vegetation types in the counties with percentages of degraded areas larger than 45%

in figure 2(a) were changed to SSiB type 9 (broadleaf shrubs with bare soil) (figure 3(b)), then the vegetation types in the counties with ratios of desertification areas larger than 30% in figure 2(b) were modified to type 11 (bare soil) (figure 3(b)), correspondingly altering the prescribed vegetation and soil properties (table 1). Vegetation maps in figures 3(a) and (b) were used in the control experiment (case C) and the degradation experiment (case D), respectively. The changes in land cover types represent the condition that may occur if the current degradation processes continue. Finally, the control experiment (case C) and the degraded experiment (case D) were conducted.

The initial conditions, lateral boundary conditions and ocean surface boundary conditions for the WRF runs in this study are given by the NCEP-DOE Reanalysis-2 (Kanamitsu *et al* 2002), hereafter NCEP R-2, at 6-h intervals. SST and sea ice were reinitialized from NCEP R-2 at the beginning of each successive 6-h simulation. The model domain was centered at 35°N and 110°E with dimensions of 196 × 154 horizontal

Table 1. June–July–August mean values of the main vegetation and soil parameters for three vegetation types.

Vegetation types	Mean surface albedo	Roughness length (m)	Mean leaf area index	Mean vegetation cover	Total soil depth (m)
Crop	0.16	0.51	6.00	0.90	3.5
Broadleaf shrubs with bare soil	0.30	0.06	0.21	0.10	1.49
Bare soil	0.32	0.01	0	0	0.49

grid points with a spacing of 30 km (figure 1). This domain covers the areas that are important for the East Asian summer monsoon (Gao *et al* 2011). The main physical packages are the WRF single-moment three-class (WSM3) microphysics scheme, the Yonsei University planetary boundary layer (YSUPBL) scheme, the Kain–Fritsch cumulus scheme, the CAM longwave and shortwave radiation scheme, and the SSiB land surface model. The models were integrated from 0000 UTC 1 March to 0000 UTC 1 September for the years 1998, 2000 and 2004, respectively. These three years were chosen because the KR D map in Xiong *et al* (2002) was interpreted from the TM satellite images of 2000. Generally, the feedbacks of land cover change to summer monsoonal climate are more significant in East Asia since most rainfall occurs in this season. Therefore, ensemble summer climate of three years integrations were used to detect the climate effects of the degraded land surface conditions and to reduce the WRF/SSiB model's noise level. The first three months (March to May) were regarded as a spin-up period and the outputs during this period were excluded from the analysis.

3. Results

3.1. Evaluation of WRF simulations

Many issues related to the downscaling capability of RCMs usually create skepticism in the application of RCMs (Castro *et al* 2005, Sato and Xue 2013), mainly because it is unclear whether the dynamic downscaling method (DDM) is really capable of adding more climate information at different scales compared to the GCM or reanalysis. On the other hand, there is uncertainty existing in the effect of LCC on the general circulation, which may cause results to be inconclusive, and sometimes even conflicting. For example, based on different climate models, Pitman *et al* (2009) found that the imposed LCC led to statistically significant decreases in the northern hemisphere summer latent heat flux in three models, but increases in three other models. Therefore, we should first assess the state-of-the-art RCM's ability to produce spatially detailed climate features for East Asia, which is the basis for realistically evaluating the LCC impact.

The Asian Precipitation-Highly Resolved Observational Data Integration towards Evaluation of the Water Resource (Yatagai *et al* 2012), called APHROD, and Global Telecommunication System (GTS), released by the World Meteorological Organization (WMO), were developed to be the state-of-the-art daily precipitation and temperature datasets, respectively, with high resolution (0.25° and 0.5°) for Asia. Thus, these two datasets were employed to assess the

Table 2. Descriptive statistics of ensemble mean JJA daily precipitation, temperature and water vapor flux at 700 hPa from WRF/SSiB and NCEP R-2 over 18°–52°N, 86°–136°E. (Note: VQ700: water vapor flux at 700 hPa ($\text{g kg}^{-1} \text{m s}^{-1}$)).

Variables		Bias	RMSE	R
Precipitation	NCEP R-2	1.95	4.22	0.60
	WRF/SSiB	1.57	3.16	0.78
Temperature	NCEP R-2	−1.93	3.62	0.86
	WRF/SSiB	−2.29	4.21	0.85
VQ700	NCEP R-2	2.89	11.38	0.65
	WRF/SSiB	−1.37	7.49	0.70

models' downscaling ability of precipitation and temperature using the ensemble average of JJA over 1998, 2000 and 2004 over 18°–52°N, 86°–136°E. In addition, the Japanese 25-year Reanalysis (JRA-25) with a spatial resolution of 1.125° (Onogi *et al* 2007) was applied to analyze the simulation performance for circulation and other atmospheric variables. Table 2 lists the statistics for precipitation and temperature from WRF/SSiB and NCEP R-2. Correlation coefficient (R), bias and root mean square error (RMSE) were applied to assess the model performance. The equations to calculate these three parameters can be found in many published materials, such as Lo *et al* (2008) and Xu *et al* (2009). The model with the lower bias and RMSE values and the higher R value means a better fit to the observations and a better model performance.

Both simulations and observations showed that most rainfall occurred in the south of China, especially south of the Yangtze River, and the temperature mainly increased from northwest to southeast, south of about 38°N, with the minimum temperature in the Qinghai-Tibetan Plateau (supplementary figure S1 available at stacks.iop.org/ERL/8/044037/mmedia). The WRF/SSiB were found to outperform NCEP R-2 in simulating precipitation, when compared with APHROD, because of the improved simulation of the low-level water vapor flux (table 2), which is a crucial factor affecting convective activity in East Asian summer monsoon. Actually, the rainfall belt and the center of maximum rainfall shown in the observations were clearer in the WRF/SSiB simulation than in NCEP R-2. Additionally, the simulation of surface temperature from WRF/SSiB was not improved over NCEP R-2 when compared with GTS, but the model presented spatial information for temperature in more detail (supplementary figure S1 available at stacks.iop.org/ERL/8/044037/mmedia), especially in the southwest and the northeast of China, and in Mongolia, which proves it is also an effective tool for downscaling temperature.

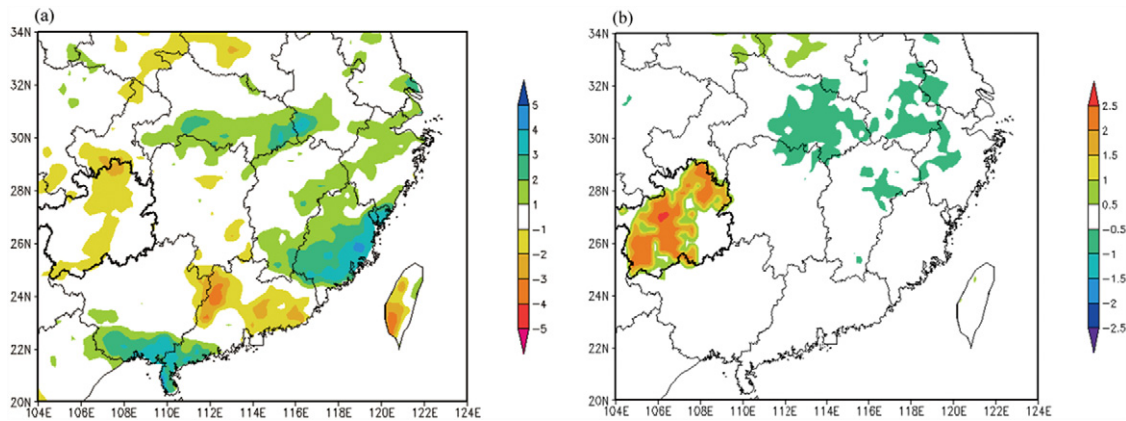


Figure 4. Ensemble mean differences in JJA (a) daily precipitation (mm/day) and (b) temperature (°C) between case D and case C. The GKP is bounded by a heavy border.

3.2. Impact of KRD on precipitation and temperature

The sensitivity study in this section just focused on the area over 20°–34°N, 104°–124°E, because the significant and consistent effects were located in this region. The changes in the precipitation varied among the regions (figure 4(a)). The simulated rainfall was reduced in the middle of the GKP and the area around 24°N, 114°E, while the simulated positive anomaly was mainly located in the middle and lower reaches of the Yangtze River and the surrounding areas. Comparatively, the simulated positive anomaly was greater in magnitude and extent. Furthermore, it should be noted that in spite of the consistent reduction of rainfall within the GKP, the variation in amplitude was not significant. Maybe this is because the abundant moisture from the Bay of Bengal weakens the impact of LCC. Contrasting with the rainfall changes, which not only occurred within the desertification area but also beyond the area, the mean surface temperature mainly increased in the GKP (figure 4(b)), especially in areas where the original vegetation types were replaced with bare soil type, as shown in figure 3(b).

3.3. Impact of KRD on surface energy balance

As shown in figure 5, the substantial changes of five components of surface energy budget occurred in the GKP. Because of the higher albedo in the degraded area (figure 5(a)), more shortwave radiation was reflected from the surface (figure 5(b)). The effect of surface albedo on the reflected shortwave radiation from the surface further influenced the surface energy balance and the surface skin temperature. The net longwave radiation at the surface was reduced (figure 5(c)) because the higher surface temperature (figure 4(b)) increased the outgoing longwave radiation. The reduction in the net shortwave and longwave radiation certainly resulted in reduced net radiation at the land surface (figure 5(d)). The warmer surface also induced more sensible heat flux (figure 5(e)), however, the increase was much less than the reduction in surface latent heat flux (figure 5(f)). The decrease in evaporation, consistent with the simulated

rainfall reductions, was partially because of the reduced net radiation, but more importantly was contributed by changes in vegetation and soil properties, such as the higher surface albedo, the lower LAI and roughness length. It is clear that, among all the components, changes in evaporation produced the most important impact on the regional hydrological balance. Actually, the above-mentioned warmer temperature occurred mainly because of the reduced evaporative cooling.

In addition, the areas with significantly changed energy budget extended beyond the GKP. Outside the degraded area, the changes in precipitation controlled the variations in surface energy partitioning into sensible and latent heat fluxes. For example, in the southeastern coastal area of China about 30°–34°N, 112°–120°E, the increase in the evaporation (figure 5(f)) was consistent with the increase in precipitation (figure 4(a)), which led to the lower temperature (figure 4(b)), as well as the lower sensible heat flux (figure 5(e)) to balance the energy budget. How the precipitation was affected by the atmospheric circulation will be discussed in section 3.4.

In order to distinguish the effects of cloud albedo on shortwave radiation from land surface albedo, we analyzed the impacts of clouds on downward shortwave radiation (figure 5(g)). Over the GKP, where the impacts were more significant, less evaporation and moisture flux convergence reduced the cloud fraction, leading to more incoming shortwave radiation. Comparatively, the increase in downward shortwave radiation was much less than the increase in upward shortwave radiation due to the higher surface albedo over the GKP (figure 5(a)); thus, the net shortwave radiation was reduced (figure 5(b)). Furthermore, from the neighboring regions of the GKP to the southeastern coastal areas of China, the increase in cloud fractions resulted in a decrease in incoming shortwave radiation, which dominated the changes in net shortwave radiation.

3.4. Impact of KRD on circulation

The above analysis of the modified water and energy balance is just the first-order effects of land degradation. The differences in heat and moisture input into the atmospheric

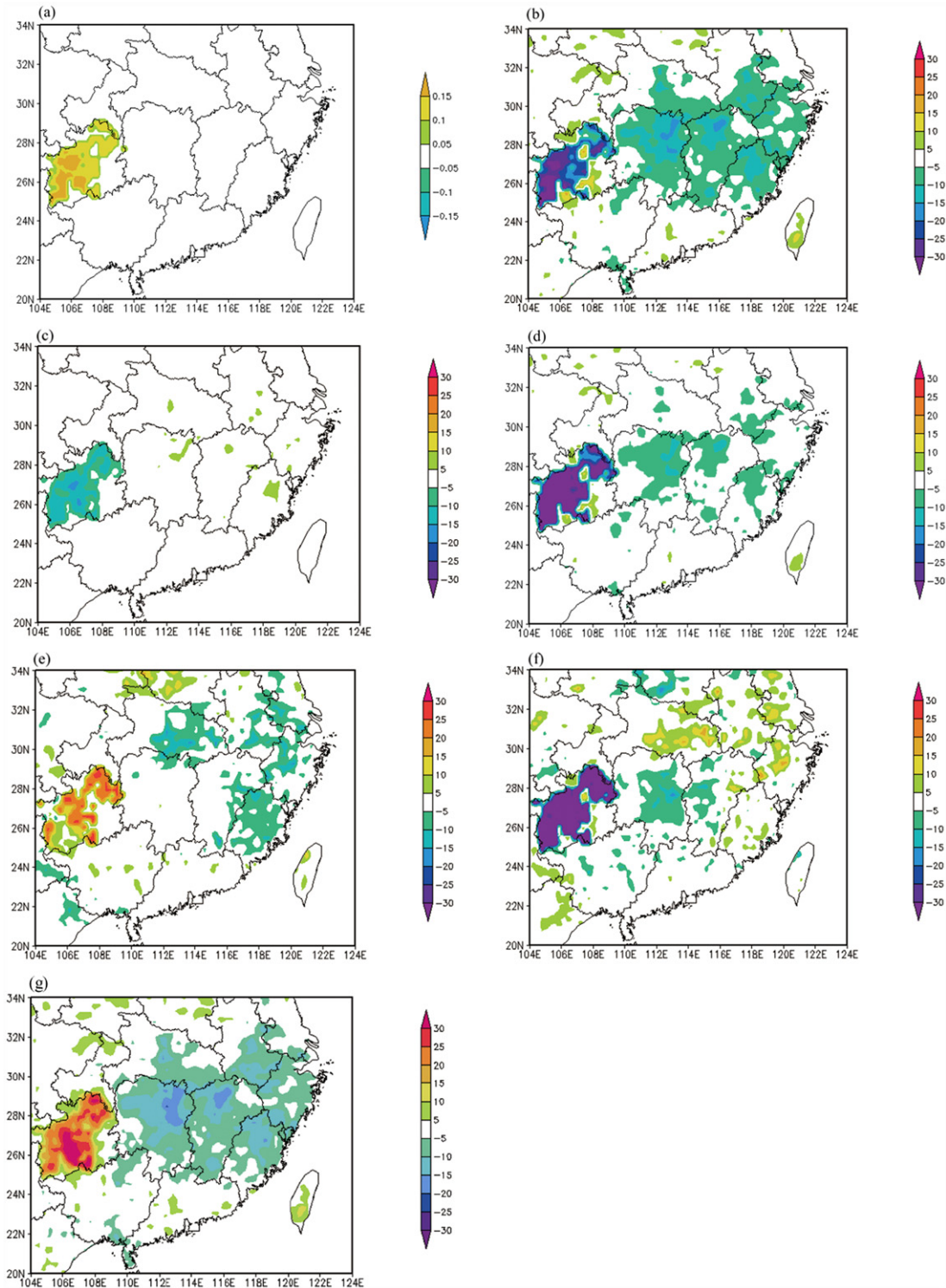


Figure 5. Ensemble mean differences in JJA (a) surface albedo, (b) net shortwave radiation, (c) net longwave radiation, (d) net radiation, (e) sensible heat flux, (f) latent heat flux, and (g) incoming shortwave radiation (W m^{-2}) between case D and case C.

boundary layer can further influence large-scale atmospheric circulation, moisture flux and precipitation beyond the desertification area. Figure 6 shows the difference of the three-month-mean wind vector at 700 hPa between case D and case C. Due to the lower surface heating in the GKP (figure 5(d)), the monsoon airflow from the Bay of Bengal,

which is an important moisture source for East Asia, was weakened from the GKP to the northeast. The result is similar to that found in Lee *et al* (2011), where they indicated that the monsoon can be weakened as potential (natural) vegetation was converted to bare ground or irrigated cropland (i.e. the decreased land surface heating). This substantial change

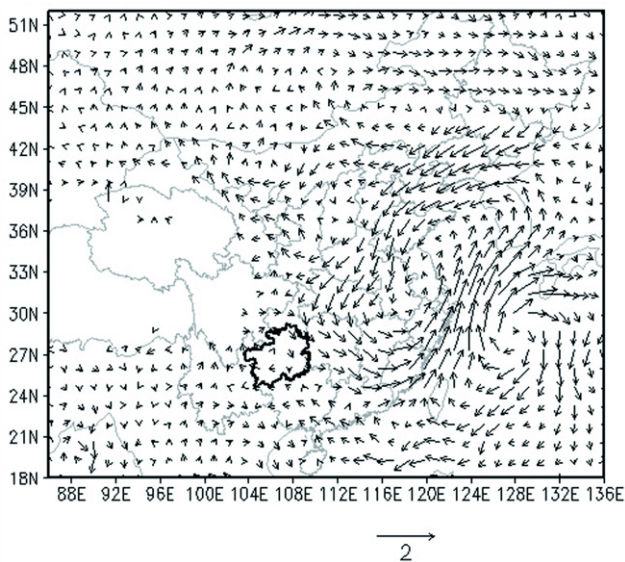


Figure 6. Ensemble mean differences in JJA wind vector (m s^{-1}) at 700 hPa between case D and case C.

would have a significant impact on the East Asian monsoon. In the southeastern coastal area, in response to the anomaly cyclone (figure 6) and the stronger horizontal convergence, the vertical ascending motion was strengthened (supplementary figure S2 available at stacks.iop.org/ERL/8/044037/mmedia), consistent with the increase in precipitation.

Figure 7 shows the longitude–height section of the composite difference of zonal circulation along 24° – 30° N between case D and case C. Corresponding to land degradation in the GKP, an anomalous descending motion appears in the upper and middle level of the troposphere over the GKP and in the middle and lower troposphere of the adjacent regions to the east. Such circulation changes resulted in the strengthened ascending motion over 114° – 122° E. Moreover, the circulation differences altered the spatial

patterns of water vapor flux. The stronger lifting over the coastal areas of southeastern China led to the increase of vertically integrated moisture flux convergence (VIMFC) from 1000 to 300 hPa. Consequently, the differences in circulation and moisture flux reduced the rainfall over the GKP and favored the formation of clouds and the positive rainfall anomalies over southeastern coastal areas (figure 4(a)). The increased amount of cloud also induced a negative net cloud-radiation forcing, which thereby may cool the surface air (figure 4(b)).

4. Conclusions and discussion

This study was designed to investigate whether the changed vegetation cover and land surface processes in the GKP are capable of modifying the summer climate simulation over East Asia using the WRF model and, if so, to explore the mechanisms in the changed land–atmosphere interactions. It indicated that KRd in the GKP led to variations in the surface energy partition into sensible and latent heat fluxes. The reduced net radiation and evaporation mainly occurred within the desertification area, accompanied by a reduction in rainfall and an increase in surface temperature. Less moisture was transferred to the atmosphere through the boundary layer for the significantly reduced evaporation. This can further result in lower diabatic heating rates, which were associated with lower moisture flux convergence and lower rainfall. The changes in precipitation in turn reduced the evaporation and convective heating, producing a positive feedback.

Similar to the study of Zuo *et al* (2011) on the LCC in the Tibet Plateau, this letter also found that the reduction in the surface heating upstream led to increased rainfall downstream. In fact, the rainfall changes beyond the desertification area were even more significant. The land–atmosphere interaction, resulting from land degradation, weakened the southwest monsoon flow and affected the atmospheric circulation and moisture flux. In the southeastern coastal areas, the

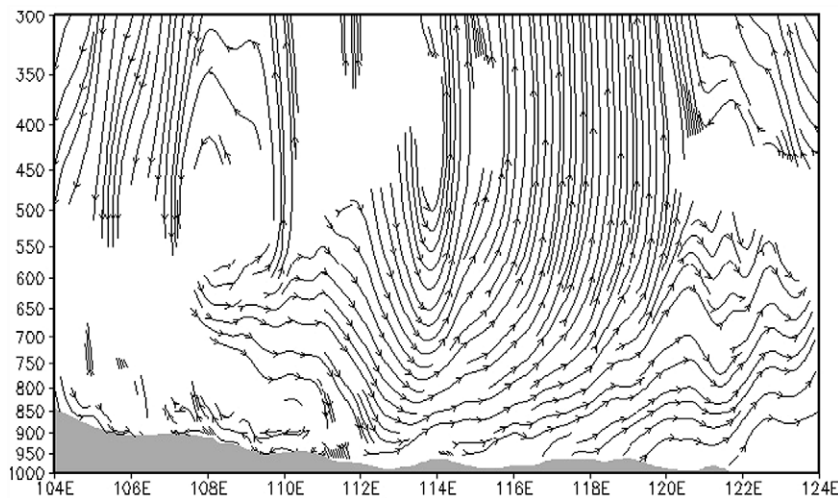


Figure 7. Zonal–height cross sections of ensemble mean differences in JJA zonal (m s^{-1}) and vertical (10^{-2} m s^{-1}) winds averaged over 24° – 30° N. Gray shading indicates topography.

weaker low-layer anti-cyclone and the enhanced horizontal convergence led to the stronger vertical ascending motion. The air mass over the GKP and neighboring regions to the east mainly sank down, diverging in the lower troposphere and rising up over southeastern China. This pattern may lead to reduced precipitation over the GKP and positive clouds anomalies with increased rainfall in coastal areas. Although such conclusions were extracted from ensemble means, the impact was similar in individual cases. The changed hydrological cycle produced a feedback on the surface energy budget, which further enhanced the changes in the heating and the vertical motion.

The SSiB vegetation map and Xiong *et al*'s research findings (2002) into the spatial distribution of different degrees of KRD worked together to determine how the land cover types were and will be changed, as well as the subsequent spatial patterns. The profound influences of land degradation over the GKP on regional climate, investigated in this letter, indicated that the fixed vegetation map in former studies on climate simulation may be unfavorable to simulating regional climate. However, the changed land surface conditions in this study are more severe than the real world. The idea is that if such a dramatic land cover change cannot produce any significant impact on regional climate, then further investigations with more realistic data would be in vain.

Several studies have pointed out that over the GKP, the vegetation cover was changed from forest/shrub to cropland, and finally to bare limestone region, in the process of KRD in cultivated land on slopes over 10°, while KRD on overgrazed land led to changed vegetation cover from grass/shrub to degraded land (i.e. reduced vegetation cover and height), and finally to desertification landscape (Wang *et al* 2003, Ren 2005); however, the related timescales have not been revealed yet because of spatial heterogeneity in the natural ecosystem and the complex mechanisms of human disturbance. In the future, based on these studies on land cover change process due to KRD, accurate and quantitative measurements of land degradation should be accessed because they are essential to further investigating this problem. Additionally, observations will be used to validate the correlations between LCC in the GKP and regional climate change. To improve the model simulation, more satellite and observation data for vegetation and soil properties will be included. The scale dependence of the impact of LCC on climate also needs to be investigated by many more numerical simulations and observations.

Acknowledgments

This work was supported by the National Natural Science Foundation of China (41301089), and the National Science and Technology Support Program of China (2012BAC19B10). The NCAR supercomputer has been used for the computations described in this letter. We thank Fernando De Sales of UCLA and Zhenxin Liu of Peking University for their helpful comments in this study.

References

- Bounoua L, Defries R, Collatz G J, Sellers P J and Khan H 2002 Effects of land cover conversion on surface climate *Clim. Change* **52** 29–64
- Castro C L, Pielke R A Sr and Leoncini G 2005 Dynamical downscaling: assessment of value retained and added using the regional atmospheric modeling system (RAMS) *J. Geophys. Res.* **110** D05108
- Gao J B, Li S C, Zhao Z Q and Cai Y L 2012 Investigating spatial variation in the relationships between NDVI and environmental factors at multi-scales: a case study of Guizhou Karst Plateau, China *Int. J. Remote Sens.* **33** 2112–29
- Gao Y H, Xue Y, Peng W, Kang H S and Waliser D 2011 Assessment of dynamic downscaling of the extreme rainfall over East Asia using a regional climate model *Adv. Atmos. Sci.* **28** 1077–98
- Gibbard S, Caldeira K, Bala G, Phillips T J and Wickett M 2005 Climate effects of global land cover change *Geophys. Res. Lett.* **32** L23705
- Huang Q H and Cai Y L 2006 Assessment of Karst rocky desertification using the radial basis function network model and GIS technique: a case study of Guizhou Province, China *Environ. Geol.* **49** 1173–9
- Kanamitsu M, Ebisuzaki W, Woollen J, Yang S K, Hnilo J J, Fiorino M and Potter G L 2002 NCEP-DOE AMIP-II reanalysis (R-2) *Bull. Am. Meteorol. Soc.* **83** 1631–43
- Lee E, Barford C C, Kucharik C J, Felzer B S and Foley J A 2011 Role of turbulent heat fluxes over land in the monsoon over East Asia *Int. J. Geosci.* **2** 420–31
- Li Q and Xue Y 2010 Simulated impacts of land cover change on summer climate in the Tibetan Plateau *Environ. Res. Lett.* **5** 015102
- Lo J C F, Yang Z L and Pielke R A Sr 2008 Assessment of three dynamical climate downscaling methods using the weather research and forecasting (WRF) model *J. Geophys. Res.* **113** D09112
- McAlpine C A, Syktus J, Deo R C, Lawrence P J, McGowan H A, Watterson I G and Phinn S R 2007 Modeling the impact of historical land cover change on Australia's regional climate *Geophys. Res. Lett.* **34** L22711
- Onogi K *et al* 2007 The JRA-25 reanalysis *J. Meteorol. Soc. Japan* **85** 369–432
- Pielke R A Sr, Avissar R, Raupach M, Dolman A J, Xeng Y and Denning S 1998 Interactions between the atmosphere and terrestrial ecosystems: influence on weather and climate *Glob. Change Biol.* **4** 461–75
- Pitman A J *et al* 2009 Uncertainties in climate responses to past land cover change: first results from the LUCID intercomparison study *Geophys. Res. Lett.* **26** L14814
- Ren H 2005 A review on the studies of desertification process and restoration mechanism of Karst rocky ecosystem *Trop. Geogr.* **25** 195–200
- Sato T and Xue Y 2013 Validating a regional climate model's downscaling ability for East Asian summer monsoonal interannual variability *Clim. Dyn.* **41** 2411–26
- Skamarock W C, Klemp J B, Dudhia J, Gill D O, Barker D, Duha M G, Huang X and Wang W 2008 *A Description of the Advanced Research WRF Version 3* NCAR/TN-475 + STR NCAR TECH NOTE
- Wang D L, Zhu S Q and Huang B L 2003 Changes of vegetation features of rocky desertification process in Karst area of Guizhou *J. Nanjing For. Univ.* **27** 26–30
- Wang S J, Liu Q M and Zhang D F 2004 Karst rocky desertification in southwestern China: geomorphology, landuse, impact and rehabilitation *Land Degrad. Dev.* **15** 115–21
- Wang Y L, Feng J M and Gao H 2013 Numerical simulation of the impact of land cover change on regional climate in China *Theor. Appl. Climatol.* doi:10.1007/s00704-013-0879-z

- Xiong K N, Li P and Zhou Z F 2002 *Typical Study on Karst Rocky-Desertification Using Remote Sensing and GIS—a Case Study in Guizhou Province* (Beijing: Geological Publishing House)
- Xu J, Rugg S, Byerle L and Liu Z 2009 Weather forecasts by the WRF-ARW model with the GSI data assimilation system in the complex terrain areas of southwest Asia *Weather Forecast.* **24** 987–1008
- Xue Y, Juang H M H, Li W P, Prince S, DeFries R, Jiao Y and Vasic R 2004 Role of land surface processes in monsoon development: East Asia and West Africa *J. Geophys. Res.* **109** D03105
- Xue Y, Sellers P J, Kinter J L and Shukla J 1991 A simplified biosphere model for global climate studies *J. Clim.* **4** 345–64
- Xue Y, Zeng F J, Mitchell K E, Janjic Z and Rogers E 2001 The impact of land surface processes on simulation of the US hydrological cycle: a case study of the 1993 flood using the SSiB land surface model in the NCEP Eta regional model *Mon. Weather Rev.* **129** 2833–60
- Yatagai A, Kamiguchi K, Arakawa O, Hamada A, Yasutomi N and Kitoh A 2012 APHRODITE: constructing a long-term daily gridded precipitation dataset for Asia based on a dense network of rain gauges *Bull. Am. Meteorol. Soc.* **93** 1401–15
- Yuan D X 1997 Rocky desertification in the subtropical karst of south China *Z. Geomorphol. N. F.* **108** 81–90
- Zhang X Z, Tang Q H, Zheng J Y and Ge Q S 2013 Warming/cooling effects of cropland greenness changes during 1982–2006 in the North China Plain *Environ. Res. Lett.* **8** 024038
- Zuo Z Y, Zhang R H and Zhao P 2011 The relation of vegetation over the Tibetan Plateau to rainfall in China during the boreal summer *Clim. Dyn.* **36** 1207–19